The 8th European Congress on Computational Methods in Applied Sciences and Engineering
ECCOMAS Congress 2022
5-–9 June 2022, Oslo, Norway

ROBUST DISCRETIZATIONS OF POROELASTICITY ENGINEERING AND MATHEMATICAL APPROACHES YOUNG RESEARCHER PRESENTATION IN PAIRS

Fleurianne Bertrand[1], Maximilian Brodbeck[2]

[1]Faculty of Electrical Engineering, Mathematics and Computer Science, University of Twente
f.bertrand@utwente.nl

[2] Institute of Mechanics, Structural Analysis and Dynamics of Aerospace Structures,
University of Stuttgart
maximilian.brodbeck@isd.uni-stuttgart.de

Key words: poroelasticity, Theory of Porous Media, FEM, flux-reconstruction

Abstract. This contribution is the proceeding of a presentation in pairs taking different viewpoints on the robustness of discretizations for poroelastic problems. These presentations are organised by the Young researcher committee to continue the tradition of fruitful interactions between applied mathematics and computational engineering. The engineering part of this contribution highlights key aspects of the theoretical framework and comments on robustness of common discretizations. Within the mathematical part of this contribution it is shown that the accurate approximation of the total stress tensor as well as the Darcy velocity are crucial to obtain reliability and robustness.

1 Introduction

Porous materials are characterized by complex interactions between the deformation of a solid skeleton and the resulting flow of an interstitial fluid. As applications of such materials range from soil mechanics up to the description of biological tissue, accurate and robust solution strategies are highly desirable. Difficulties arise, as model constants vary over wide ranges and might lead to locking, when nearly incompressible solids are considered, or pressure oscillations for low permeablilities.

Poroelasticity is commonly described either by the theory of Biot as introduced in [1], Mixture Theory (MT, see [2]) or the Theory of Porous Media (TPM, see [3, 4]). While Biot derived a saddle-point problem from a phenomenological viewpoint, MT and TPM are based on the homogenization of mixtures alongside with a thermodynamically consistent modeling of arising interaction terms. These formulations usually consider the solid displacement and the fluid pressure as primal variables. However, the accurate approximation of total stress tensor as well as Darcy velocity is crucial to obtain reliable and robust approximations, see [5]. Since standard methods do not lead to $H(div)$-conforming stresses and fluxes, surface or interface traction forces resp. fluid fluxes cannot be evaluated. Recovering strategies are outlined in [6, 7, 8].

Within this contribution we will give a short overview over the description of porous materials within the framework of the TPM and introduce some common discretization schemes. Based on the footing problem – a common test-case for consolidation processes – we will discuss influences of impermeability on different discretization schemes and highlight inaccuracies of standard schemes when it comes to flux quantities. Thereby motivated, we will outline the recovery of stress- and flux quantities as well as their relevance in the construction of reliable error estimators.

2 Governing equations

Porous materials consist of α different constituents, which are statistically distributed over the complete control space of a continuum. Following De Boer [3] and Ehlers and Bluhm [4] the real micro-structure can be homogenized such that every material point $\mathbf{X}_\alpha$ within reference placement Ω_0 is occupied by all phases. Their spacial distribution is given by the volume factions n^α, describing the relation of the different partial volumes:

$$\mathrm{n}^\alpha = \frac{\mathrm{dv}^\alpha}{\mathrm{dv}}, \quad \sum_{\alpha=1}^{\kappa} \mathrm{n}^\alpha = 1\,. \tag{1}$$

Considering $\kappa = 2$ immiscible and incompressible phase – $\alpha = \mathrm{S}$ denotes a solid, $\alpha = \mathrm{F}$ a fluid – each phase has its own motion. They can described by explicitly capturing the deformation of the solid and a constitutive assumption for the relative kinematic of both phases $\mathbf{w}_{\mathrm{FS}} = \mathbf{x}'_{\mathrm{F}} - \mathbf{x}'_{\mathrm{S}}$.

As the homogenized porous material is simply the mixture of interacting constituents, its over all field equations are based on the balance equations of mass, moment and moment of momentum of each phase $\alpha \in \{\mathrm{F}, \mathrm{S}\}$

$$(\mathrm{n}^\alpha)'_\alpha + \mathrm{n}^\alpha \nabla_{\mathbf{x}} \cdot \left(\mathbf{x}'_\alpha\right) = 0,\ \nabla_{\mathbf{x}} \cdot \mathbf{T}^\alpha + \rho^\alpha \mathbf{b} = \hat{\mathbf{p}}^\alpha,\ \mathbf{T}^\alpha = (\mathbf{T}^\alpha)^T\ . \tag{2}$$

In eq. (2), $\mathbf{T}^\alpha$ denotes the Cauchy stress, ρ^α the partial density and $\hat{\mathbf{p}}^\alpha$ a source term due to interactions of fuid and solid. Summation over both phases yields the overall balance laws for the mixture in current configuration:

$$\nabla_{\mathbf{x}} \cdot \left[\mathbf{x}'_{\mathrm{S}}\right] + \nabla_{\mathbf{x}} \cdot \left[\mathrm{n}^{\mathrm{F}} \mathbf{w}_{\mathrm{FS}}\right] = 0,\ \nabla_{\mathbf{x}} \cdot \mathbf{T} + \left(\rho^{\mathrm{F}} + \rho^{\mathrm{S}}\right) \mathbf{b} = \mathbf{0},\ \mathbf{T} = \mathbf{T}^T\ . \tag{3}$$

To close eqs. (3), constitutive relations for the total stress tensor $\mathbf{T}$ and seepage velocity $\mathrm{n}^{\mathrm{F}} \mathbf{w}_{\mathrm{FS}}$ are required. Within the following we will assume a hyper-elastic behaviour of the solid matrix and consider Darcy's law for the description of the relative velocity between fluid and solid. Pull-back into reference configuration Ω_0 and the assumption of small deformation leads, to

$$\nabla_{\mathbf{X}} \cdot \left[\mathbf{x}'_{\mathrm{S}}\right] + \nabla_{\mathbf{X}} \cdot \left[\mathrm{n}^{\mathrm{F}} \mathbf{w}_{\mathrm{FS}}|_{0\mathrm{S}}\right] = 0,\ \nabla_{\mathbf{X}} \cdot \left[\boldsymbol{\sigma}^{\mathrm{SE}} - \mathrm{p}\, \mathbf{h}_1\right] = \mathbf{0}\ , \tag{4}$$

$$\begin{gathered} \mathbf{h}_1 = (1 + \nabla_{\mathbf{X}} \cdot \mathbf{u})\, \mathrm{I} - 2\boldsymbol{\varepsilon}_{\mathrm{S}},\ \mathrm{n}^{\mathrm{F}} \mathbf{w}_{\mathrm{FS}}|_{0\mathrm{S}} = -\mathrm{k}_{\mathrm{D}} \nabla_{\mathbf{X}}\, \mathrm{p}\, \mathbf{h}_1, \\ \boldsymbol{\sigma}^{\mathrm{SE}} = 2\mu^{\mathrm{S}} \boldsymbol{\varepsilon}_{\mathrm{S}} + \lambda^{\mathrm{S}} \nabla_{\mathbf{X}} \cdot \mathbf{u} \end{gathered} \tag{5}$$

a set of partial differential equations, typically solved for the primal field quantities displacement and pressure. This linearization of the TPM is hereafter abbreviated as lTPM. Biot's equations – assuming a Biot-Willis coefficient a = 1 and vanishing storage $\mathrm{Q} \to \infty$ – can be recovered from eqs. (4, 5), by choosing $\mathbf{h}_1 = \mathrm{I}$. Subsequently they may be interpreted as a solution to the balance equations in the actual placement, assuming a linear stress-strain relation.

3 Weak forms and discretization

Constructing discretization methods for poroelastic problems, it is generally possible to start from different sets of primal variables. No matter which, two fundamental aspects has to be considered: To guaranty existence, uniqueness and stability, each field quantity has to be approximated in appropriate function spaces. For coupled problems, this typically requires the fulfillment of appropriate conditions of the Inf-Sub type. Additionally to theses fundamental requirements, the wide range of possible model constants makes parameter independent convergence properties – what is typically referred to as robustness – favourable. In terms of convergence theory this would require the Cea's constant in an a-priory error estimate to be independent of the spacial discretization parameter h as well as the model parameters.

Within the following, discretizations of eqs. (4, 5) based on different primal variables – namely displacement-pressure ($\mathbf{u}-\mathrm{p}$) and displacement-velocity-pressure ($\mathbf{u}-\mathbf{v}_\mathrm{D}-\mathrm{p}$) – will be introduced. Arising time derivatives are captured by a backward differentiation formula of order 1 (BDF1). For the sake of simplicity, the weak forms are given for the Biot system but can be extended to the lTPM.

3.1 The $\mathbf{u}-\mathrm{p}$ formulation

Find $(\mathbf{u},\, p) \in \mathbf{H}^1 \times \mathrm{H}^1$ such that

$$\begin{aligned} a^1(\mathbf{u},\, \mathbf{v_u}) + b^1(\mathrm{p}, \mathbf{v_u}) &= l^1(\mathbf{v_u}) \\ b^1(\mathrm{v_p}, \mathbf{u}) + a^2(\mathrm{p},\, \mathrm{v_p}) &= l^2(\mathrm{v_p}) \end{aligned} \tag{6}$$

holds for all test-function $(\mathbf{v_u},\, \mathrm{v_p}) \in \mathbf{H}^1 \times \mathrm{H}^1$. Let Ω_0 be the reference placement and $\Gamma \subseteq \partial\Omega_0$, then linear and bilinear forms are defined in the following way

$$\begin{gathered} a^1(\mathbf{u},\, \mathbf{v_u}) = \int 2\mu^\mathrm{S}\, \boldsymbol{\varepsilon}_\mathrm{S} \cdot \nabla_\mathbf{X} \mathbf{v_u} + \lambda^\mathrm{S}\, \nabla_\mathbf{X} \cdot \mathbf{u}\, \nabla_\mathbf{X} \cdot \mathbf{v_u}\, \mathrm{d}\Omega_0, \quad b^1(\mathrm{p}, \mathbf{v_u}) = -\int \mathrm{p}\, \nabla_\mathbf{X} \cdot \mathbf{v_u}\, \mathrm{d}\Omega_0 \\ l^1(\mathbf{v_u}) = \int \mathbf{T} \cdot \mathbf{v_u}\, \mathrm{d}\Gamma \end{gathered} \tag{7}$$

$$a^2(\mathrm{p},\, \mathrm{v_p}) = -\int \mathrm{k_D} \Delta\mathrm{t}\, \nabla_\mathbf{X} \mathrm{p} \cdot \nabla_\mathbf{X} \mathrm{v_p}\, \mathrm{d}\Omega_0, \quad l^2(\mathrm{v_p}) = \int (\nabla_\mathbf{X} \cdot \mathbf{u}^n)\, \mathrm{v_p}\, \mathrm{d}\Omega_0 + \int \mathrm{v_{D,bc}}\, \mathrm{v_p} \mathrm{d}\Gamma \tag{8}$$

while the fluid flux over the boundary is defined by

$$\mathrm{v_{D,bc}} = \mathrm{n^F}\, \mathbf{w}_\mathrm{FS}|_{0\mathrm{S}} \cdot \mathbf{n}\,. \tag{9}$$

Displacement and pressure are typically approximated, using Lagrangian elements. While equal order (EO) approximations are possible, so-called Taylor-Hood (TH) elements, where the approximation order for the displacement $k+1$ is one order higher than that for the pressure, are more common. Uniform convergence rates with respect to the permeability can only be achieved using the latter ones.

3.2 The $\mathbf{u} - \mathbf{v}_\mathrm{D} - \mathrm{p}$ formulation

Within this three-field formulation an additional field quantity for the seepage velocity

$$\mathbf{v_D} = -\mathrm{k_D} \nabla_\mathbf{X} \mathrm{p} \tag{10}$$

is introduced. The resulting equation system is given in eq. (11). The additional variable for the fluid flux, allows for discontinuous pressure approximations. Choosing $(\mathbf{u},\, \mathbf{v}_\mathrm{D},\, \mathrm{p}) \in \mathbf{H}^1 \times \mathrm{H(div)} \times \mathrm{L}^2$, the weak form eq. (12) has to be fulfilled for all test-functions $(\mathbf{v_u},\, \mathbf{w},\, \mathrm{v_p}) \in \mathbf{H}^1 \times \mathrm{H(div)} \times \mathrm{L}^2$.

$$\begin{aligned} \nabla_\mathbf{X} \cdot \left[\boldsymbol{\sigma}^\mathrm{SE} - \mathrm{p}\,\mathbf{I}\right] &= \mathbf{0} \\ \Delta\mathrm{t}\, {\mathrm{k_D}}^{-1} \mathbf{v}_\mathrm{D} + \Delta\mathrm{t} \nabla_\mathbf{X} \mathrm{p} &= \mathbf{0} \\ \nabla_\mathbf{X} \cdot \left[\mathbf{x}'_\mathrm{S}\right] + \nabla_\mathbf{X} \cdot \left[\mathbf{v}_\mathrm{D}\right] &= 0 \end{aligned} \tag{11}$$

$$\begin{aligned} a^1(\mathbf{u},\, \mathbf{v_u}) - b(\mathbf{v_u},\, \mathrm{p},) &= l^1(\mathbf{v_u}) \\ a^2(\mathbf{v}_\mathrm{D},\, \mathbf{w}) - \Delta\mathrm{t} \cdot b(\mathbf{w},\, \mathrm{p}) &= l^2(\mathbf{w}) \\ -b(\mathbf{u}, \mathrm{v_p}) - \Delta\mathrm{t} \cdot b(\mathbf{v}_\mathrm{D},\, \mathrm{v_p}) &= l^3(\mathrm{v_p}) \end{aligned} \tag{12}$$

Let Ω_0 be the reference placement and $\Gamma \subseteq \partial\Omega_0$, then linear and bilinear forms are defined in the following way:

$$a^1(\mathbf{u},\, \mathbf{v_u}) = \int 2\mu^\mathrm{S}\, \boldsymbol{\varepsilon}_\mathrm{S} \cdot \nabla_\mathbf{X} \mathbf{v_u} + \lambda^\mathrm{S}\, \nabla_\mathbf{X} \cdot \mathbf{u}\, \nabla_\mathbf{X} \cdot \mathbf{v_u}\, \mathrm{d}\Omega_0, \quad l^1(\mathbf{v_u}) = \int \mathbf{T} \cdot \mathbf{v_u}\, \mathrm{d}\Gamma \tag{13}$$

$$a^2(\mathbf{v}_\mathrm{D},\, \mathbf{w}) = \int \Delta\mathrm{t}\, {\mathrm{k_D}}^{-1}\, \mathbf{v}_\mathrm{D},\, \mathbf{w}\, \mathrm{d}\Omega_0, \quad l^2(\mathbf{w}) = -\int \mathrm{p}\, \mathbf{n} \cdot \mathbf{w}\, \mathrm{d}\Gamma \tag{14}$$

$$b(\mathbf{u}, \mathrm{v_p}) = \int \nabla_\mathbf{X} \cdot \mathbf{u}\, \mathrm{v_p}\, \mathrm{d}\Omega_0, \quad l^3(\mathrm{v_p}) = -\int (\nabla_\mathbf{X} \cdot \mathbf{u}^n)\, \mathrm{v_p}\, \mathrm{d}\Omega_0 \tag{15}$$

The classical discretization method – combining Lagrangian elements (order $k = 2$) with an $\mathrm{RT}_0 \times \mathcal{P}_0$ pair – is analysed in Mardal et al. [9]. This method will be used for calculations presented in section 4.1. Even if it is beyond the scope of this contribution, a point-wise mass-conserving and fully parameter robust discretization based on this formulation is achievable. Following the concepts of parameter-independent stability by Lee at al. [10], Kraus et al. [11, 12] used H(div)-conforming displacement spaces, alongside with an appropriate Raviart-Thomas pair for the flow-sub-problem. These methods are easily scalable in approximation order and result in linear equation system comparable in size to those, arising from the $\mathbf{u} - \mathrm{p}$ formulation.

4 Numerical example: The footing test

As outlined within the previous sections, the fluid flux is one of the most important quantities within the description of poroelastic materials. Following eq. (4), it can be directly calculated from the pressure gradient and the permeability $\mathrm{k_D}$. Accurate pressure approximations are therefore indispensable for accurate fluid fluxes. Introducing a time discretization based on the BDF1, the numerical time step $\Delta\mathrm{t}$ is an additional influence factor on the flow sub-problem. Subsequently impermeability has to be seen in relation of either small time steps or small possibilities. Based on the footing problem we will discuss the influence of small effective possibilities $\tilde{\mathrm{k}}_\mathrm{D} = \Delta\mathrm{t}\, \mathrm{k_D}$ on pressure. Furthermore the fluid fluxes, post-processed from the pressure gradient at the integration points, will be compared with the directly approximated dual quantity. The observed inaccuracies are one part of the motivation for recovery technique's of flux quantities.

4.1 Case setup

The footing test describes the consolidation of a rectangular domain, which is partially loaded on the top surface. Geometry as well as the naming convention of the boundary surfaces are given in figure 1. For all subsequent calculations the domain is fixed ($\mathbf{u} = \mathbf{0}$) on surface Γ_3 while a traction boundary condition

$$\boldsymbol{\sigma} = \boldsymbol{\sigma}^{\mathrm{SE}} - \mathrm{p}\,\mathbf{h}_1,\ \boldsymbol{\sigma}\cdot\mathbf{n} = -10\times 10^4\,\mathrm{N\,m^{-2}}$$

is applied on Γ_1. Furthermore outflow boundary conditions ($\mathrm{p} = 0$) are applied on $\Gamma_{2,3}$, while the outflow is prevented on Γ_1. Material parameters used within the presented calculation are given in table 1.

$\mathrm{E^S}$	ν^{S}	$\mathrm{k_D}$	$\mathrm{n^S_{0S}}$
$3\times 10^4\,\mathrm{N\,m^{-2}}$	0.4995	$1\times 10^{-12}\,\mathrm{m^3\,s^2\,kg^{-1}}$	0.5

Table 1: Material parameters of the footing problem

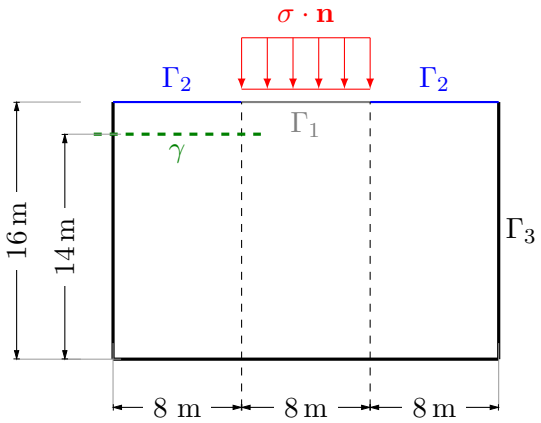

Figure 1: Footing problem: Undeformed domain and definition of the boundary surfaces.

4.2 Influence of impermeability

Based on the work of Favino et al. [13], a minimum time step $\Delta\mathrm{t}_{min}$, above which pressure oscillations are prevented, can be calculated based on the assumption of a 2D domain, TH elements of order $k = 1$, and $\mu^{\mathrm{S}} \ll \lambda^{\mathrm{S}}$:

$$\Delta\mathrm{t}_{min} = \frac{h_{ref}^2}{3\mathrm{k_D}\,\lambda^{\mathrm{S}}}\,. \tag{16}$$

No further assumption on. e.g. boundary conditions are necessary. If the assumption on the Lamé parameters does not hold, significantly larger time steps are possible before pressure oscillation occur. Based on the material parameters in table 1 and a mesh size of $h_{ref} = 0.5\,\mathrm{m}$,

oscillation-free solutions can be achieved if $\Delta t > 8339\,\mathrm{s}$. For a systematic comparison, a time factor

$$f_t = \frac{\Delta t_{min}}{\Delta t} \tag{17}$$

is defined. For $f_t > 1$ pressure oscillations occur. As depicted within figure 2, these are (at first) located near the outflow boundaries, as they induce steep pressure gradients. Using a discretization based on the $\mathbf{u} - \mathrm{p}$ formulation and TH elements, these pressure oscillations stay confined near the boundary and are nearly constant in magnitude, even if the time step is significantly reduced (compare figure 2 (a)).

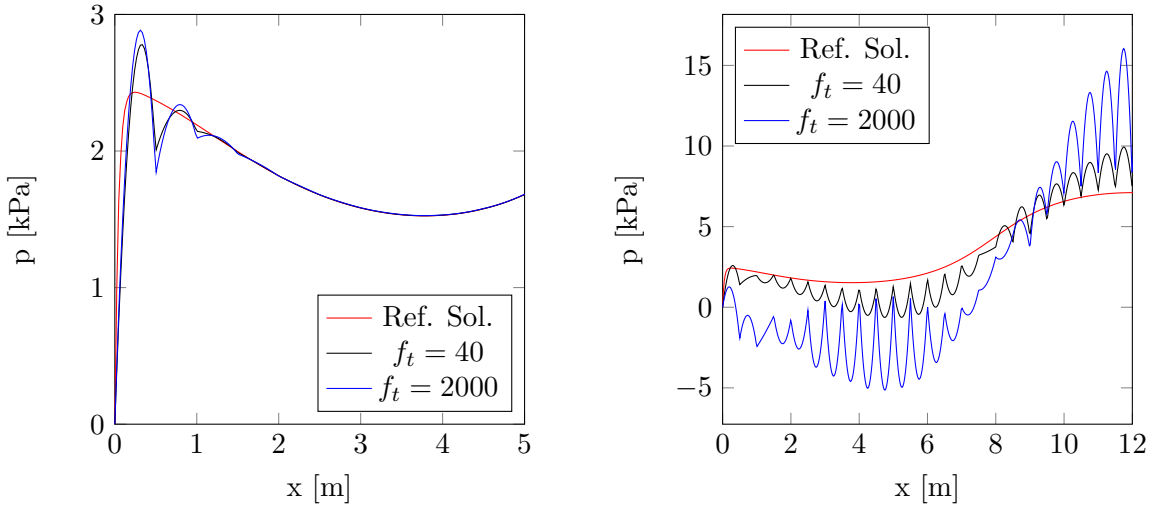

Figure 2: Pressure distribution ($\mathrm{t} = \Delta \mathrm{t}$) over γ for the $\mathbf{u} - \mathrm{p}$ formulation using (a) TH elements of order $k = 2$ and (b) EO elements of order $k = 2$.

A quite different behaviour can be observed when EO discretizations are applied. Chessboard-like pressure distribution occur (compare figure 2 (b)) while the magnitudes of the spurious pressure modes are amplified for increasing f_t. Increasing the approximation order k decreases the oscillations but can not fully prevent them, if the effective permeability $\tilde{\mathrm{k}}_{\mathrm{D}}$ is further reduced. EO discretizations are therefore clearly more prone to pressure oscillations than discretizations based on TH elements.

So far we have only considered the initial time step of the test-case. Within the subsequent time steps, pressure oscillations decay, as it was proven by Murad and Loula [14, 15] for Biot's equations. This also holds for finite element spaces, which are not Stokes stable (e.g. EO discretizations for displacement and pressure). Even tough Inf-Sub stable finite element pairs can not fully prevent pressure oscillations, they typically hinder their increase with decreasing effective permeability. This is of practical interest, particularly when the short-term behaviour in presence of transient boundary conditions shall be studied (see e.g. Stokes et al. [16]).

4.3 Flux accuracy

In the last section pressure oscillations within the standard $\mathbf{u} - \mathrm{p}$ formulations in the nearly impermeable limit were discussed. It seems obvious, that fluid fluxes calculated from pressure fields containing spurious pressure modes can not yield acceptable results. Alternatives are provided by formulations, which directly approximate the fluid flux. As it was shown in section 3.2, such formulations are typically based on discontinuous pressure approximations and a weak consideration of Dirichlet boundary conditions on the pressure field.

For a comparison of fluid fluxes, gained from a post-processing of the pressure field with the direct approximation of the dual quantity, a footing test with $f_t = 0.5$ is considered. Subsequently no spurious pressure oscillations occur, which could distort the comparison. Figure 3 shows the pressure profile over γ as well as the fluid flux over the right vertical boundary. While the accuracy of the directly approximated fluid fluxes is even on course meshes ($h = 0.5\,\mathrm{m}$) quite satisfactory (compare figure 3 (b)), the pressure field does not match the prescribed boundary condition $\mathrm{p} = 0$ (compare figure 3 (a)). With decreasing mesh size, the boundary conditions can

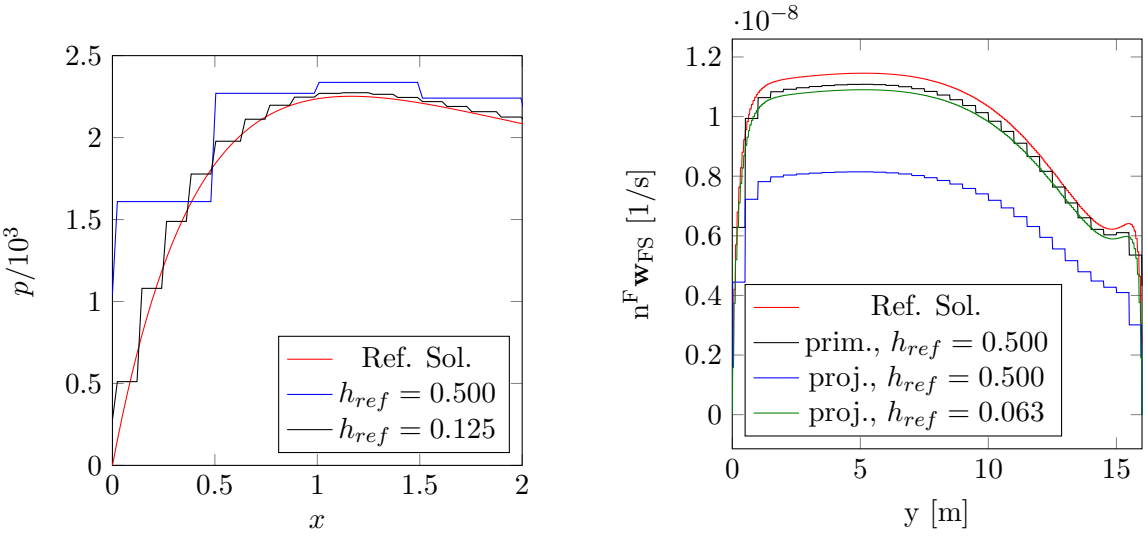

Figure 3: (a) Pressure distribution ($\mathrm{t} = \Delta\mathrm{t}$) over γ for the $\mathbf{u} - \mathbf{v}_{\mathrm{D}} - \mathrm{p}$ formulation and (b) comparison of reconstructed fluid fluxes ($\mathrm{t} = \Delta\mathrm{t}$) based on the $\mathbf{u} - \mathrm{p}$ formulation (proj) and the primal calculated flux (prim) using $f_t = 0.5$

be fulfilled. Focusing now on the fluid fluxes calculated based on the $\mathbf{u} - \mathrm{p}$ formulation, by projection between integration points and the element nodes, the initial fluid flux over the boundary is significantly underestimated. As it can be seen from figure 3 (b), that an 8 times finer mesh is required to gain projected fluxes, that are comparable to their direct approximation.

5 Reconstruction of the $H(div)$-quantities

Let us state again that the motivation to recover $H(div)$-quantities from discontinuous approximation is two-fold. One one hand, accurate representation are crucial in many application,

in particular to evaluate surface tension forces. On the other hand, the difference between the recovered $H(div)$-quantity to the corresponding discontinuous approximation provides a reliable error estimator.

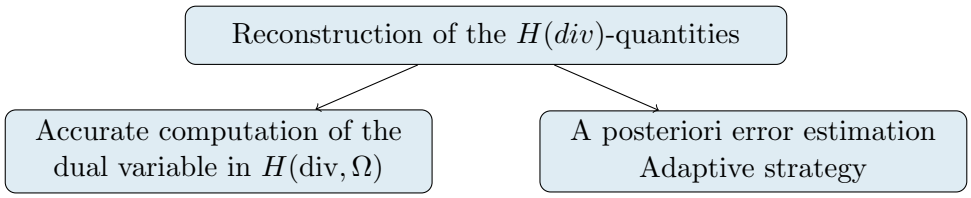

Figure 4: Motivation for Reconstruction of the $H(div)$-quantities

For the porous media discretisations introduced in the previous sections 2, recall that the pressure p is sought in $H^1_{\Gamma_D}(\Omega)$ but for the purpose of the exposition, assume that it is smooth enough to define div ∇p. However, while the discrete pressure $p_h \in H^1_{\Gamma_D}(\Omega)$ is continuous over the edge of the triangulation $\mathcal{T}$ but its gradient is discontinuous with respect to the triangulation $\mathcal{T}$. The key idea of the equilibration strategy is the following identity dating back to [17]: for any $\mathbf{w} \in H_{\Gamma_N}(\mathrm{div}, \Omega)$ with div $\mathbf{w} =$ div ∇p,

$$\|\nabla p - \nabla p_h\|^2 + \|\nabla p - \mathbf{w}\|^2 = \|\nabla p_h - \mathbf{w}\|^2 \ , \tag{18}$$

holds. Expanding the terms on the right side, the proof relies on the fact that the mixed term $(\nabla p - \nabla p_h, \nabla p - \mathbf{w})$ vanishes. Indeed,

$$(\nabla(p - p_h), \nabla p - \mathbf{w}) = -(p - p_h, \text{div } \nabla p - \text{div } \mathbf{w}) \ + \langle p - p_h, \nabla p - \mathbf{w} \rangle = 0 \ .$$

Note that the integration by parts also leads to $(\nabla p, \mathbf{w}) = -(\text{div } \mathbf{w}, p) = (\nabla p, \nabla p)$, i.e

$$(\nabla p, \nabla p - \mathbf{w}) = 0 \ .$$

Similarly $(\nabla p, \nabla p_h) = -(\text{div} \nabla p, v)$ and $(\mathbf{w}, \nabla p_h) = -(\text{div } \mathbf{w}, p_h)$ and thus

$$(\nabla p - \mathbf{w}, \nabla p_h) = 0 \ . \tag{19}$$

With the foot $\widehat{\mathbf{w}}$ of ∇p_h on the hyperplane defined by (19) it holds

$$(\nabla p - \widehat{\mathbf{w}}, \nabla p - \mathbf{w}) = 0 \ .$$

The segment connecting $\mathbf{w}$ to $\widehat{\mathbf{w}}$ is therefore the diameter of the hypercircle Γ, whose center is denoted by C in Figure 5. To visualise the effect of the reconstruction in $H(\mathrm{div}, \Omega)$, an example is given in Figure 6.

It remains to construct such a $\mathbf{w}$ locally. A possible construction is given in [18], where the authors construct the difference $\mathbf{w}^\Delta = \mathbf{w} - \nabla p_h$ in the discontinuous Raviart thomas spaces, such that

$$\text{div } \mathbf{w}^\Delta = \text{div } \nabla p - \text{div } \nabla p_h \tag{20}$$

$$[\![\mathbf{w}^\Delta \cdot \mathbf{n}]\!]_E = -[\![\nabla p_h \cdot \mathbf{n}]\!]_E \tag{21}$$

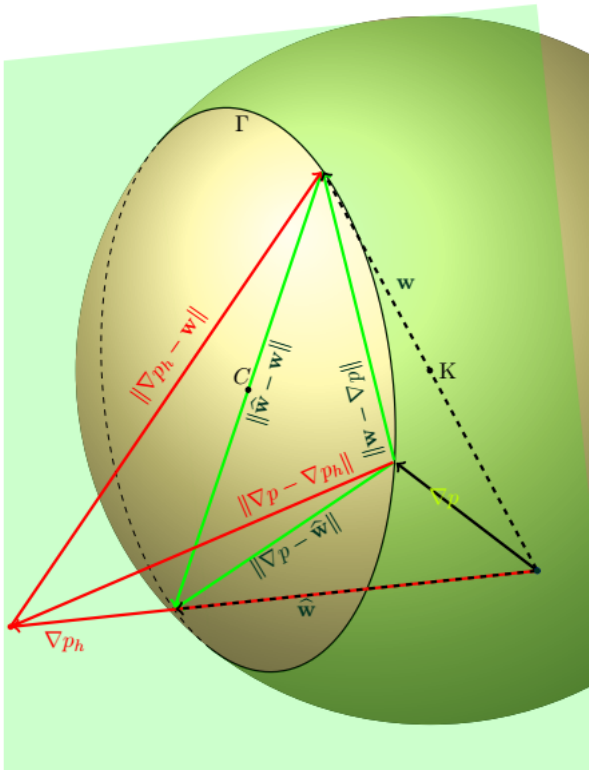

Figure 5: Hypercircle notations

holds. Exploiting some basic properties of the Raviart–Thomas finite element spaces, these conditions can be realised with a local post-processing. Note that this is also a particular application of the analysis provided in [19], where extensions of piecewise polynomial data prescribed on faces of a patch of simplices sharing a vertex are studied (see also [19, 20]. It leads directly to an error estimator and the optimal convergence rates of the adaptive algorithm is proved in [21].

6 Reconstruction of symmetric $H(div)$ stress tensors

For the description of the porous media, the theory introduced in the previous section needs to be extended to problems involving symmetric gradients, such that linear elasticity [8], or hyperelasticity [7, 22]. One possibility is to reconstruct the stresses in the symmetric Arnold-Winter space. This type of reconstruction allows for an immediate application of the theory of the previous section but the finite element space is significantly more complicated than the Raviart-Thomas space. Another possibility therefore consists in a weakly symmetric reconstruction. However, the fact that the reconstructed stress is not pointwise symmetric implies that a measure for its asymetry has to enter the error estimator. Indeed, rewriting equation (18) leads to

$$\|\boldsymbol{\varepsilon}(v) - \mathcal{A}\sigma\|^2 = \|\boldsymbol{\varepsilon}(u - v)\|^2 + \|\boldsymbol{\varepsilon}(u) - \mathcal{A}\sigma\|^2 + 2\,(\boldsymbol{\varepsilon}(u - v), \boldsymbol{\varepsilon}(u) - \mathcal{A}\sigma) \tag{22}$$

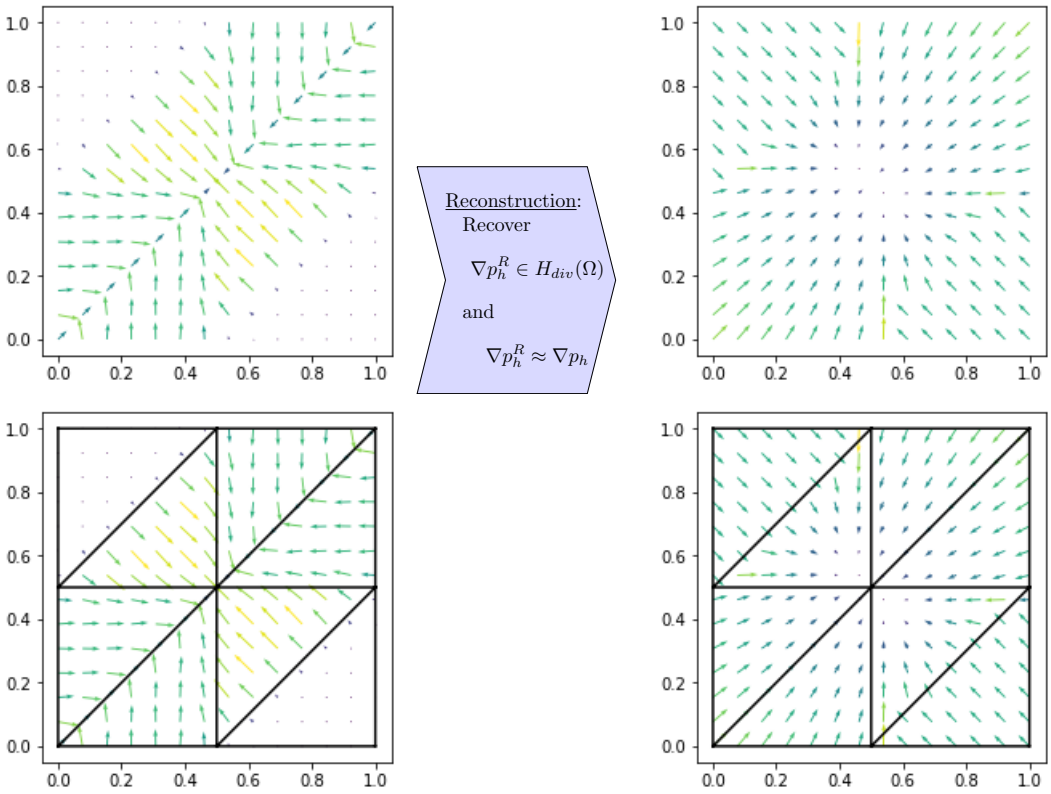

Figure 6: Example of reconstruction

for any $u, v \in (H^1_{\Gamma_D}(\Omega))^d$ and $\sigma \in (H_{\Gamma_N}(\mathrm{div}, \Omega))^d$. The presence of the symmetric gradient in the mixed term prevents the integration by parts to cancel the mixed term. On possibility is to split the symmetric gradient $\boldsymbol{\varepsilon}(u - v)$ of the mixed term into it full-gradient and its assymetric part, i.e.

$$\begin{aligned} \|\boldsymbol{\varepsilon}(v) - \mathcal{A}\sigma\|^2 &= \|\boldsymbol{\varepsilon}(u - v)\|^2 + \|\boldsymbol{\varepsilon}(u) - \mathcal{A}\sigma\|^2 + 2\left(\nabla(u - v), \boldsymbol{\varepsilon}(u) - \mathcal{A}\sigma - \mathbf{as}(\boldsymbol{\varepsilon}(u) - \mathcal{A}\sigma)\right) \quad (23) \\ &= \|\boldsymbol{\varepsilon}(u - v)\|^2 + \|\boldsymbol{\varepsilon}(u) - \mathcal{A}\sigma\|^2 + 2\left(\nabla(u - v), \boldsymbol{\varepsilon}(u) - \mathcal{A}\sigma + \mathbf{as}(\mathcal{A}\sigma)\right) \quad (24) \end{aligned}$$

With the appropriate equilibration condition, the first part of the mixed term vanishes after the integration by parts, i.e. $(\nabla(u - v), \boldsymbol{\varepsilon}(u) - \mathcal{A}\sigma +) = 0$, and it remains

$$\begin{aligned} \|\boldsymbol{\varepsilon}(v) - \mathcal{A}\sigma\|^2 &= \|\boldsymbol{\varepsilon}(u - v)\|^2 + \|\boldsymbol{\varepsilon}(u) - \mathcal{A}\sigma\|^2 + 2\left(\nabla(u - v), \boldsymbol{\varepsilon}(u) - \mathcal{A}\sigma - \mathbf{as}(\boldsymbol{\varepsilon}(u) - \mathcal{A}\sigma)\right) \quad (25) \\ &= \|\boldsymbol{\varepsilon}(u - v)\|^2 + \|\boldsymbol{\varepsilon}(u) - \mathcal{A}\sigma\|^2 + 2\left(\nabla(u - v), \mathbf{as}(\mathcal{A}\sigma)\right) \ . \quad (26) \end{aligned}$$

With the Korn constant C_K, we obtain

$$2(\mathbf{as}\,\sigma, \nabla(u - v)) \leq 2C_K \|\mathbf{as}\,\sigma\| \, \|\boldsymbol{\varepsilon}(u - v)\| \leq \frac{C_K^2}{\delta} \|\mathbf{as}\,\sigma\|^2 + \delta \|\boldsymbol{\varepsilon}(u - v)\|^2 \,, \quad (27)$$

for any $\delta > 0$. Of course, in order to use these estimates in an a posteriori setting, a global Korn constant should be avoided. In fact, it is possible to derive these estimates locally, using a local Korn constant, if σ is weakly symmetric, see [8].

This combination of the reconstruction for flux and stresses is crucial for adaptive computations in porous media, see [6].

7 Conclusion and Outlook

Within this contribution we discussed robustness and accuracy of gradient dependent quantities, based on standard discretizations. We showed that solution of the lTPM, based on the $\mathbf{u}-\mathrm{p}$ formulation in combination with Stokes-unstable finite element spaces, exhibit strong pressure oscillations in early time-steps which amplifies, for deceasing permeability. Even if pressure oscillations are prevented by sufficient time steps, flux quantities projected from interpolation to nodal points were shown to be of insufficient accuracy.

This is one part of the motivation for $H(div)$-conforming reconstructions of fluid flux and total stress. Based on the outlined strategy, this can be done locally, avoiding the expensive solution of large linear equation systems. Beside their increased accuracy, these flux quantities can serve as basis for robust a posteriori error estimators and adaptive solution strategies.

At the current point, robust disctretization strategies as well as reconstructions were mainly derived for Biot's theory. Within our future work we intent to transfer these techniques to the TPM, a theoretical framework who's advantage is the capturing of the non-linear nature of realistic applications.

8 Acknowledgement

This contribution demonstrates that collaborations between mathematicians and engineers are crucial for the progresses in the development of solution strategies for challenging problems. We therefore are grateful for the work of the young investigator community of the Eccomas for the possibility of the research in pairs presentations and for allowing us to speak in those exceptional minisymposia. The authors thanks their respective mentor Tim Ricken and Gerhard Starke for fruitful discussions.

References

[1] M. A. Biot. "General Theory of Three-Dimensional Consolidation". In: *Journal of Applied Physics* 12.2 (1941), pp. 155–164.

[2] R. Bowen and J. Wiese. "Diffusion in mixtures of elastic materials". In: *International Journal of Engineering Science* 7.7 (1969), pp. 689–722.

[3] R. De Boer. *Theory of porous media: highlights in historical development and current state.* Springer Science & Business Media, 2012.

[4] W. Ehlers and J. Bluhm. *Porous media: theory, experiments and numerical applications.* Springer Science & Business Media, 2002.

[5] F. Bertrand and M. Brodbeck. "On robust discretization methods for poroelastic problems: Numerical examples and counter-examples". In: *submitted to EXCO* (2022).

[6] F. Bertrand and G. Starke. “A posteriori error estimates by weakly symmetric stress reconstruction for the Biot problem”. English. In: *Computers and mathematics with applications* 91 (June 2021), pp. 3–16. ISSN: 0898-1221.

[7] F. Bertrand, M. Moldenhauer, and G. Starke. “Weakly symmetric stress equilibration for hyperelastic material models”. In: *GAMM Mitteilungen* 43.2 (2020).

[8] F. Bertrand et al. “Equilibrated Stress Reconstruction and a Posteriori Error Estimation for Linear Elasticity”. In: *Computers and mathematics with applications* 597 (2020), pp. 69–106.

[9] K.-A. Mardal, M. E. Rognes, and T. B. Thompson. “Accurate discretization of poroelasticity without Darcy stability”. In: *BIT Numerical Mathematics* (Mar. 2021).

[10] J. J. Lee, K.-A. Mardal, and R. Winther. “Parameter-Robust Discretization and Preconditioning of Biot’s Consolidation Model”. In: *SIAM Journal on Scientific Computing* 39.1 (2017), A1–A24.

[11] Q. Hong and J. Kraus. “Parameter-robust stability of classical three-field formulation of Biot’s consolidation model”. In: *ETNA - Electronic Transactions on Numerical Analysis* 48 (2018), pp. 202–226.

[12] J. Kraus et al. “Uniformly well-posed hybridized discontinuous Galerkin/hybrid mixed discretizations for Biot’s consolidation model”. In: *Computer Methods in Applied Mechanics and Engineering* 384 (2021), p. 113991.

[13] M. Favino, A. Grillo, and R. Krause. “A Stability Condition for the Numerical Simulation of Poroelastic Systems”. In: *Poromechanics V*, pp. 919–928.

[14] M. A. Murad and A. F. Loula. “Improved accuracy in finite element analysis of Biot’s consolidation problem”. In: *Computer Methods in Applied Mechanics and Engineering* 95.3 (1992), pp. 359–382.

[15] M. A. Murad and A. F. D. Loula. “On stability and convergence of finite element approximations of Biot’s consolidation problem”. In: *International Journal for Numerical Methods in Engineering* 37.4 (1994), pp. 645–667.

[16] I. A. Stokes et al. “Limitation of Finite Element Analysis of Poroelastic Behavior of Biological Tissues Undergoing Rapid Loading”. In: *Annals of Biomedical Engineering* 38.5 (May 2010), pp. 1780–1788. ISSN: 1573-9686.

[17] W. Prager and J. L. Synge. “Approximations in elasticity based on the concept of function space”. In: *Quart. Appl. Math.* 5 (1947), pp. 241–269.

[18] D. Braess and J. Schöberl. “Equilibrated residual error estimator for edge elements”. In: *Math. Comp.* 77 (2008), pp. 651–672.

[19] A. Ern and M. Vohralík. “A posteriori error estimation based on potential and flux reconstruction for the heat equation”. In: *SIAM J. Numer. Anal.* 48 (2010), pp. 198–223.

[20] A. Ern and M. Vohralík. “Polynomial-degree-robust a posteriori error estimates in a unified setting for conforming, nonconforming, discontinuous Galerkin, and mixed discretizations”. In: *SIAM J. Numer. Anal.* 53 (2015), pp. 1058–1081.

[21] F. Bertrand and D. Boffi. “The Prager-Synge theorem in reconstruction based a posteriori error estimation”. In: 75^{th} *Mathematics of Computation, Contemporary Mathematics* volume 754 (2019).

[22] F. Bertrand, M. Moldenhauer, and G. Starke. “Stress Equilibration for Hyperelastic Models”. In: *Lecture Notes in Applied and Computational Mechanics* 98 (2022), pp. 91–105.